# Numerical Analysis of Sparse-Array Metasurface Antennas using Gaussian Basis Functions

Jonathan Dessy, *Student Member, IEEE,* Modeste Bodehou, *Member, IEEE,*
and Christophe Craeye, *Senior Member, IEEE*

***Abstract*—A sparse-array metasurface (MTS) antenna corresponds to a continuously modulated sheet impedance on top of a grounded slab, periodically repeated over many unit cells (with a few wavelengths cell size). The structure is fed with an array of surface-wave (SW) feeds placed at the center of each cell. Such structures may be used to provide continuous beam scanning with a sparse feeding network. Given the larger unit cell and the large number of scan angles to be considered, the computation of the embedded element pattern (EEP) in such array may be very intensive. This paper proposes an accelerated Method of Moment (MoM) tool allowing the efficient analysis of EEPs of modulated MTSs with periodic boundary conditions (PBC). To that aim, the unknown current distribution as well as the sheet impedance are expanded into a set of regularly spaced Gaussian basis functions. The sheet impedance expansion is carried out efficiently using the fast Fourier transform (FFT) algorithm. The adopted Gaussian functions along with the mesh regularity are also employed to dramatically accelerate the MoM matrix computation using FFT-based methods. Numerical results are validated with that from the commercial software HFSS.**

***Index Terms*—Method of Moments, Gaussian, periodic, sparse array, phased array, metasurface, FFT.**

## I. Introduction

SURFACE-WAVE (SW) based metasurface (MTS) antennas have received a great attention over the past fifteen years [1]–[3]. They are made of a thin grounded dielectric slab on which subwavelength metal patterns are periodically arranged [1], [4], [5]. An integrated feeder generates a SW that can produce radiation through leaky waves due to its interaction with the MTS layer [6], [7]. Their numerical analysis is typically based on solving Maxwell's equations in their surface-integral form with the Method of Moments (MoM) [8]–[11]. In this method, the MTS layer can be homogenized and accurately modeled as a spatially modulated sheet imposing impedance boundary conditions (IBC) on top of the dielectric slab [9], [10]. The MoM relies on the surface equivalence principle and links the radiated fields to the surface currents through the Green's function [12]–[14].

This work was supported in part by a Research Fellow (ASP) grant from the Belgium Fonds National de la Recherche Scientifique (F.R.S.-FNRS); and in part by the HORIZON EUROPE EIC Pathfinder Open programme under grant agreement No. 101098996 "Flexible intelligent near-field sensing skins (FITNESS)". Funded by the European Union. Views and opinions expressed are however those of the author(s) only and do not necessarily reflect those of the European Union. Neither the European Union nor the granting authority can be held responsible for them. J. Dessy and C. Craeye are with the ICTEAM Institute, Université catholique de Louvain (UCLouvain), 1348 Louvain-la-Neuve, Belgium (e-mail: jonathan.dessy@uclouvain.be; christophe.craeye@uclouvain.be). M. Bodehou is with the Ecole Polytechnique d'Abomey-Calavi, Université d'Abomey-Calavi (UAC), 01 BP 2009, Cotonou, Benin (e-mail: modeste.bodehou@uac.bj).

In the present paper, we are interested in the analysis of the embedded element pattern (EEP) of sparse-array MTS antennas, modeled as a sheet impedance that is periodically modulated along the $x$ and $y$ directions. The considered cell size is of the order of a few wavelengths. In each cell, a SW launcher feed is placed in the slab and an arbitrary phase shift can be imposed in the periodic boundary conditions (PBC), as shown in Fig. 1. In a later instance, each cell may be implemented with an array of sub-wavelength patches, as illustrated in Fig. 1(b). This type of structure can be used to provide continuous beam scanning with a sparse-array feeding network [15]. The EEP corresponds to the pattern radiated by the entire structure for excitation of the reference feed only. This requires the simulation of the MTS with PBC for each direction of observation, with the appropriate phase shift [16]. Such a periodic structure can be analyzed very efficiently with the well-known periodic MoM [13], [14], [17]–[19], which is already popular to study the radiation of a unit cell patch with PBC [4], [6]. However, as the EEP simulation requires the solutions of many periodic problems (with a large unit cell), the total computation time may become significant. In this respect, this paper addresses the effective analysis of a modulated surface impedance with PBC in a cell with size of the order of a few wavelengths. The work is a 3-D extension of the methodology presented in [20], which was restricted to the 2-D MoM formulation. Regularly spaced Gaussian basis functions are proposed to expand the current distribution as well as the sheet impedance modulation, due to their spatial and spectral filtering property. As will be shown, this choice of basis functions enables an efficient fast Fourier transform (FFT)-based expansion of the sheet impedance, as well as an FFT-based acceleration of the periodic MoM matrix computation. Those acceleration techniques are new and were not presented in [20]. Acceleration methods based on the FFT have already been exploited with other types of basis functions, such as rooftop basis functions in [21], [22].

The paper is structured as follows. Section II presents the considered structure and the periodic MoM analysis. Section III describes how the MoM matrix can be efficiently computed with FFT-based acceleration techniques. Finally, Section IV shows validation results and provides the computational savings of the algorithm. Conclusions are drawn in Section V.

## II. Periodic Method of Moments formulation

Let us consider a modulated MTS with PBC, as illustrated in Fig. 1. The modulated MTS is modeled as a sheet impedance distribution laying on a grounded dielectric slab of relative permittivity $\epsilon_r$ and thickness $d_{slab}$. The cell size is $a$ along $x$, and $b$ along $y$. In each cell, the feeder is modeled as a vertical elementary dipole (VED), with unitary amplitude, placed in the center of the cell and in the middle of the substrate ($z = -d_{slab}/2$) [6], [23]. Given the PBC, the analysis can

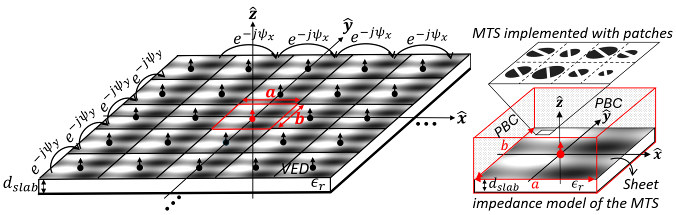


(a) (b)

Fig. 1. Modulated MTS with PBC and impressed phase shifts $-\psi_x$ and $-\psi_y$ along $x$ and $y$, respectively. (a) infinite structure. (b) reference cell and feed.

be restricted to a single reference cell (see the red cell in Fig. 1) with the periodic MoM [13], [14], [17]–[20]. The latter should be solved for many phase shifts to generate the desired EEP [16]. The unknown surface current distribution (flowing on the sheet) associated with the reference cell is decomposed into a weighted sum of $N$ basis functions along each direction:

$$\boldsymbol{J}(x,y) = \sum_{n=1}^{N} F_b^n(x,y)\,(i_n^x\,\hat{\boldsymbol{x}} + i_n^y\,\hat{\boldsymbol{y}}), \tag{1}$$

where $i_n^x$ and $i_n^y$ are the weights associated with the $n$-th basis function $F_b^n$ oriented along $x$ and $y$, respectively. In this work, the basis functions are chosen as regularly spaced Gaussian functions defined as

$$F_b^n(x,y) = \frac{1}{2\pi\sigma_x\sigma_y}\, e^{-\frac{(x-\mu_{x,n})^2}{2\sigma_x^2} - \frac{(y-\mu_{y,n})^2}{2\sigma_y^2}}, \tag{2}$$

where $\sigma_{x/y}$ and $\mu_{x/y,n}$ denote the width and the position of the $n$-th basis function along $x/y$, respectively. The basis functions are centered on a regular rectangular grid of size $N_{\mu_x} \times N_{\mu_y}$, with $N_{\mu_x} N_{\mu_y} = N$. This class of basis functions admits a closed-form Fourier transform (FT) given by

$$\tilde{F}_b^n(k_x,k_y) = e^{j(k_x\mu_{x,n} + k_y\mu_{y,n})}\, e^{-\frac{\sigma_x^2 k_x^2 + \sigma_y^2 k_y^2}{2}}, \tag{3}$$

where $k_x$ and $k_y$ are the spectral Cartesian coordinates. Gaussian functions have been chosen due to their filtering property, both in space and spectral domains. In particular, this choice will offer several acceleration opportunities for establishing the MoM linear system of equations. Those accelerations were not presented in [20] and are detailed in Section III. The spatial filtering of the basis functions will also make it easier to extend the analyzed structures to more general MTS shapes. After inserting (1) into the electric field integral equation (EFIE) and testing the fields with the same basis functions, one obtains the following MoM linear system of equations [9], [11]:

$$\left(\begin{bmatrix} \boldsymbol{Z_G^{xx}} & \boldsymbol{Z_G^{xy}} \\ \boldsymbol{Z_G^{yx}} & \boldsymbol{Z_G^{yy}} \end{bmatrix} - \begin{bmatrix} \boldsymbol{Z_{IBC}^{xx}} & \boldsymbol{Z_{IBC}^{xy}} \\ \boldsymbol{Z_{IBC}^{yx}} & \boldsymbol{Z_{IBC}^{yy}} \end{bmatrix}\right) \begin{bmatrix} \boldsymbol{i^x} \\ \boldsymbol{i^y} \end{bmatrix} = \begin{bmatrix} \boldsymbol{v^x} \\ \boldsymbol{v^y} \end{bmatrix}, \tag{4}$$

where $\boldsymbol{Z_G}$ is the substrate MoM matrix, $\boldsymbol{Z_{IBC}}$ is the IBC MoM matrix, $\boldsymbol{i}$ is the current coefficients vector, and $\boldsymbol{v}$ is the excitation vector. Each matrix is composed of 4 submatrices defined by the polarization of the considered testing and basis functions (first and second exponent, respectively). It can be shown that their expressions are given by [9], [13], [19]

$$\begin{aligned} Z_G^{xy}(m,n) = \frac{1}{ab} \sum_{p=-\infty}^{+\infty} \sum_{q=-\infty}^{+\infty} \tilde{F}_b^{n,y}(k_x^p,k_y^q) \\ \tilde{G}^{xy}(k_x^p,k_y^q)\, \tilde{F}_t^{m,x}(-k_x^p,-k_y^q), \end{aligned} \tag{5}$$

$$\begin{aligned} Z_{IBC}^{xy}(m,n) = \sum_{u=-\infty}^{+\infty} \sum_{v=-\infty}^{+\infty} e^{-j(\psi_x u + \psi_y v)} \int_{-\infty}^{+\infty}\int_{-\infty}^{+\infty} \\ F_b^{n,y}(x-ua,y-vb)\, Z_s^{xy}(x,y)\, F_t^{m,x}(x,y)\, dx\, dy, \end{aligned} \tag{6}$$

$$v^x(m) = \frac{-1}{ab} \sum_{p=-\infty}^{+\infty} \sum_{q=-\infty}^{+\infty} \tilde{E}_i^x(k_x^p,k_y^q)\, \tilde{F}_t^{m,x}(-k_x^p,-k_y^q), \tag{7}$$

where $F_t^{m,x}$ denotes the $m$-th $x$-oriented testing function, $\tilde{G}^{xy}$ is the substrate spectral Green's function associated with the $x$-oriented electric field and the $y$-oriented current [24], [25], $Z_s^{xy}$ is the sheet transition impedance model of the MTS associated with the $x$-oriented electric field and $y$-oriented current, $\tilde{E}_i^x$ is the $x$-oriented spectral incident electric field associated with the VED excitation. Finally, $k_x^p = \psi_x/a + p2\pi/a$ and $k_y^q = \psi_y/b + q2\pi/b$ are the Floquet wavenumbers associated with the impressed phase shifts $-\psi_x$ and $-\psi_y$ along $x$ and $y$, respectively. The expression of the other submatrices can be easily deduced from the previous ones. The summations in (5) and (7) converge relatively fast owing to the spectral filtering of the Gaussian functions.

## III. Periodic Method of Moments computation

### A. Impedance Boundary Condition Matrix

Because of the arbitrary impedance profile in the reference cell, the IBC matrix has no special structure. However, thanks to the adopted Gaussian shape of the basis and testing functions, and depending on the size of the reference cell, many interactions can be neglected, resulting in a sparse IBC matrix. As the product of Gaussian functions remains Gaussian and analytically integratable, each of the 4 components of the sheet impedance tensor is approximated as a weighted sum of Gaussian basis functions. In this way, the IBC matrix can be evaluated extremely fast, in closed form. Given the periodicity of the impedance profile, the impedance basis functions are placed on a regular rectangular grid on the reference cell and are periodically repeated in the other cells. For example, the $xy$ component of the impedance profile is approximated as

$$\begin{aligned} Z_s^{xy}(x,y) \approx \sum_{m=-\infty}^{+\infty} \sum_{n=-\infty}^{+\infty} \sum_{p=\frac{-N_x}{2}}^{\frac{N_x}{2}-1} \sum_{q=\frac{-N_y}{2}}^{\frac{N_y}{2}-1} h_{p,q}^{xy} \\ g\left(x - ma - pa/N_x, y - nb - qb/N_y\right), \end{aligned} \tag{8}$$

where $g(x,y)$ is the reference Gaussian function (centered at the origin), $h^{xy}$ is a sampled function whose values correspond to the weights of the Gaussian functions, and $N_x$ and $N_y$ denote the number of Gaussian functions in the reference cell along $x$ and $y$, respectively. The spatial sampling frequency is chosen so as to satisfy the sampling theorem [26], according to the bandwidth of $Z_s^{xy}$. Considering that the Gaussian functions are not orthogonal, the impedance profile expansion requires in principle the construction and the inversion of a linear system of equations. However, it can be shown that, in this case, an appropriate choice for the unknown values is given by

$$h_{p,q}^{xy} = \frac{ab}{N_x N_y} \sum_{t=\frac{-N_x}{2}}^{\frac{N_x}{2}-1} \sum_{u=\frac{-N_y}{2}}^{\frac{N_y}{2}-1} \frac{s_{t,u}^{xy}\, e^{j2\pi\left(\frac{tp}{N_x}+\frac{uq}{N_y}\right)}}{\tilde{g}(k_x = t\frac{2\pi}{a}, k_y = u\frac{2\pi}{b})}, \quad (9)$$

where $\tilde{g}$ is the analytical FT of the reference Gaussian function, and $s_{t,u}^{xy}$ corresponds to the coefficients of the Fourier series expansion of $Z_s^{xy}$. The latter can be computed efficiently with the FFT algorithm. It is worth observing that (9) has the structure of a 2-D FT. As a consequence, it can be computed extremely fast with the FFT algorithm. Equation (9) can be understood as follows. The goal is to find a sampled and periodic function $h^{xy}$ so that, after convolution with the reference Gaussian function $g$, a good approximation of $Z_s^{xy}$ is obtained. In spectral domain, the convolution turns into a product between $\tilde{h}^{xy}$ and $\tilde{g}$. Due to the not strictly limited bandwidth of $\tilde{g}$, this product is not exactly band-limited, and therefore, cannot provide the exact FT of $Z_s^{xy}$, as illustrated in Fig. 2. The proposed decomposition is thus not exact but can still be sufficiently accurate for well-chosen Gaussian widths (e.g. $a/N_x$ and $b/N_y$ along $x$ and $y$, respectively). An appropriate choice for the unknown samples of $h^{xy}$ can be obtained as the inverse FT of the ratio between $\tilde{Z}_s^{xy}$ and $\tilde{g}$, which is mathematically reflected as (9). This approach is similar to the popular Whittaker–Shannon interpolation scheme [26], [27], but enables the use of relatively local basis functions in both domains. Once the impedance profile is expanded into a Gaussian basis, each element of $\boldsymbol{Z_{IBC}}$ can be expressed as a sum of integrals of Gaussian functions. The latter integrals are separable along $x$ and $y$, and can be evaluated analytically using the following identity:

$$\int_{-\infty}^{+\infty} e^{-(a_x x^2 + b_x x + c_x)}\, dx = \sqrt{\frac{\pi}{a_x}}\, e^{\frac{b_x^2}{4a_x} - c_x}, \quad (10)$$

where $a_x > 0$, $b_x$ and $c_x$ are the corresponding coefficients.

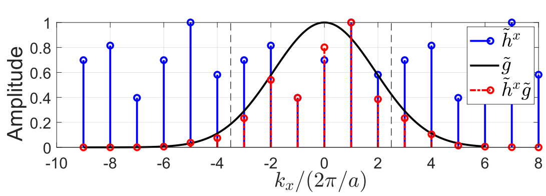


Fig. 2. The approximated impedance spectrum (shown in red) is not strictly limited to the desired bandwidth, bounded by the dashed lines.

## B. Substrate Matrix

Inserting (3) into (5) (with $\tilde{F}_b^n = \tilde{F}_t^n$), one obtains

$$Z_G^{xy}(m,n) = \frac{1}{ab} \sum_{p=-\infty}^{+\infty} \sum_{q=-\infty}^{+\infty} e^{j(k_x^p \Delta\mu_{x,mn} + k_y^q \Delta\mu_{y,mn})} \underbrace{\tilde{G}^{xy}(k_x^p, k_y^q)\, e^{-\sigma_x^2 (k_x^p)^2 - \sigma_y^2 (k_y^q)^2}}_{\tilde{B}^{xy}(k_x^p, k_y^q)}, \quad (11)$$

with $\Delta\mu_{x/y,mn} = \mu_{x/y,n} - \mu_{x/y,m}$. It can be observed that each entry of the submatrix only depends on the difference between the location of the testing and basing functions, rather than on their absolute locations. As the basis functions are located on a regular rectangular grid, the submatrix has a Toeplitz-block Toeplitz structure composed of $N_{\mu_x} \times N_{\mu_x}$ blocks of size $N_{\mu_y} \times N_{\mu_y}$, resulting in a linear matrix filling complexity. Further investigation of the submatrix shows that elements can be efficiently computed all at once using the FFT algorithm, as done in [21] and [22] with rooftop basis functions. Indeed, after truncating the summations and setting $\Delta\mu_{x,mn} = \alpha_{mn}\, a/N_{\mu_x}$ and $\Delta\mu_{y,mn} = \beta_{mn}\, b/N_{\mu_y}$ where $\alpha_{mn} \in\ ]-N_{\mu_x}, N_{\mu_x}[$ and $\beta_{mn} \in\ ]-N_{\mu_y}, N_{\mu_y}[$ are integers, (11) simplifies to

$$Z_G^{xy}(m,n) = \frac{1}{ab} e^{j\left(\frac{\psi_x \alpha_{mn}}{N_{\mu_x}} + \frac{\psi_y \beta_{mn}}{N_{\mu_y}}\right)} \sum_{p=-p_{max}}^{p_{max}-1} \sum_{q=-q_{max}}^{q_{max}-1} \tilde{B}^{xy}(k_x^p, k_y^q)\, e^{j2\pi\left(\frac{p\alpha_{mn}}{N_{\mu_x}} + \frac{q\beta_{mn}}{N_{\mu_y}}\right)}, \quad (12)$$

which has the form of a 2-D FT if $2\,p_{max} \propto N_{\mu_x}$ and $2\,q_{max} \propto N_{\mu_y}$. Thus, (12) can be computed at once for all $\alpha_{mn}$ and $\beta_{mn}$ using a single 2-D FFT. Of course, this FFT-based approach requires $p_{max}$ and $q_{max}$ to be appropriately chosen such that $2\,p_{max} \propto N_{\mu_x}$ and $2\,q_{max} \propto N_{\mu_y}$, and such that the spectral summation in (12) converges (at a rate depending on the width of the Gaussian functions).

## C. Excitation Vector

Inserting (3) into (7) (with $\tilde{F}_b^n = \tilde{F}_t^n$) yields

$$v^x(m) = \frac{-1}{ab} \sum_{p=-\infty}^{+\infty} \sum_{q=-\infty}^{+\infty} e^{-j(k_x^p \mu_{x,m} + k_y^q \mu_{y,m})} \underbrace{e^{-\frac{\sigma_x^2 (k_x^p)^2 + \sigma_y^2 (k_y^q)^2}{2}}\, \tilde{E}_i^x(k_x^p, k_y^q)}_{\tilde{C}^x(k_x^p, k_y^q)}. \quad (13)$$

After truncating the summations and setting $\mu_{x,m} = -a/2 + \alpha_m\, a/N_{\mu_x}$ and $\mu_{y,m} = -b/2 + \beta_m\, b/N_{\mu_y}$ where $\alpha_m \in [0, N_{\mu_x}[$ and $\beta_m \in [0, N_{\mu_y}[$ are integers, one gets

$$v^x(m) = \frac{-1}{ab} e^{\frac{j}{2}(\psi_x + \psi_y)}\, e^{-j\left(\frac{\psi_x \alpha_m}{N_{\mu_x}} + \frac{\psi_y \beta_m}{N_{\mu_y}}\right)} \sum_{p=-p_{max}}^{p_{max}-1} \sum_{q=-q_{max}}^{q_{max}-1} \tilde{C}^x(k_x^p, k_y^q)\, e^{j\pi(p+q)}\, e^{-j2\pi\left(\frac{p\alpha_m}{N_{\mu_x}} + \frac{q\beta_m}{N_{\mu_y}}\right)}, \quad (14)$$

which has the same form as (12). Thus, all entries of the excitation subvector can be computed at once with a 2-D FFT.

# IV. Simulation Results

First, the proposed algorithm is validated using the commercial software HFSS. To that aim, the MTS antenna depicted in Fig. 1 is considered, with an operating frequency of 24 GHz. The dielectric slab has a relative permittivity $\epsilon_r = 3.66$ and a thickness $d_{slab} = 1.524$ mm. The MTS is considered isotropic and modeled as a sheet impedance given by

$$Z_s(x, y) = jX_0 \left(1 + M \sin(k_0 x) + M \sin(2k_0 y)\right), \quad (15)$$

where $X_0 = -1200\,\Omega$ is the average impedance, $M = 0.4$ is the modulation depth, and $k_0 = 2\pi/\lambda_0$ is the free-space wavenumber, with $\lambda_0$ being the free-space wavelength at the operating frequency. The cell size is fixed to $2\lambda_0 \times 2\lambda_0$. The embedded aperture electric field, i.e. the aperture field generated after exciting the reference feed only, is computed with our periodic MoM code, following the procedure described in [16]. The result is compared with that of the commercial software HFSS. It is worth mentioning that for the HFSS simulation, we have not used PBC, but a large MTS of finite size ($6\lambda_0 \times 6\lambda_0$), obtained after repeating many unit cells. The sheet impedance has been sampled using cells of size $\lambda_0/10 \times \lambda_0/10$. The feed is modeled as an infinitesimal vertical current source and radiation conditions have been added at the rim to avoid field reflection due to the finite size of the antenna. Convergence of the result with a larger MTS and a finer sampling of the impedance has been checked to ensure the validity of the solution. The obtained $x$-directed aperture electric field is compared with that of HFSS in Fig. 3. A very good agreement is obtained with HFSS, thus validating our code. The computational time with our code is now analyzed.

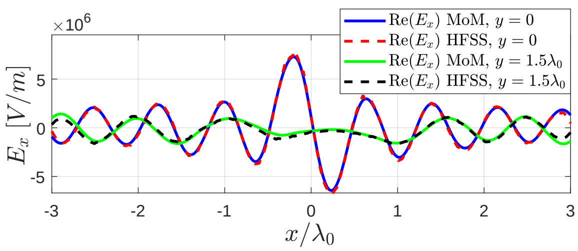


Fig. 3. $x$-directed embedded aperture electric field obtained with HFSS (finite MTS) and with our MoM code (infinite MTS) at $y = 0$ and $y = 1.5\lambda_0$.

For a given applied phase shift and different cell sizes, the computation times required to build the MoM matrix and the excitation vector are compared with those of the brute-force implementation in Table I. The code has been implemented

TABLE I
MoM COMPUTATION TIMES REQUIRED WITH THE PROPOSED METHOD COMPARED WITH THOSE OF THE BRUTE-FORCE IMPLEMENTATION.

| Cell size / Number of unknowns | | $\lambda_0 \times \lambda_0$ / 200 | $2\lambda_0 \times 2\lambda_0$ / 800 | $3\lambda_0 \times 3\lambda_0$ / 1800 |
|---|---|---|---|---|
| $\boldsymbol{Z_{IBC}}$ | Brute-force | 385 ms | 3 s | 11.4 s |
| | Accelerated | 45 ms | 400 ms | 1.4 s |
| $\boldsymbol{Z_G}$ | Brute-force | 30 ms | 270 ms | 1.1 s |
| | Accelerated | 1.5 ms | 5 ms | 19 ms |
| $\boldsymbol{v}$ | Brute-force | 7 ms | 65 ms | 280 ms |
| | Accelerated | 0.5 ms | 1.5 ms | 2.7 ms |
| Matrix inversion | | 0.6 ms | 8 ms | 63 ms |

in MATLAB R2023a and runs on a conventional desktop computer equipped with an Intel Core i7 CPU and 32 GB of RAM. The Toeplitz-block Toeplitz structure of the substrate matrix and the sparsity of the IBC matrix have been exploited in both implementations (accelerated and brute-force). Therefore, the difference between both implementations relies solely on the usage of FFT techniques. It can be observed that the usage of the FFT dramatically accelerates the matrix filling computation. This acceleration is particularly convenient for the study of EEPs, as the periodic MoM should be called for each direction of observation. In that case, further acceleration techniques can be adopted, such as precomputing only once the IBC matrix interactions between the testing and shifted basis functions without any phase shift, and applying the appropriate phase shift in (6) for each direction of interest. Thus, the bottleneck of the algorithm lies in the computation of the elements of $\boldsymbol{Z_G}$ whose complexity has been reduced from $\mathcal{O}(N^2)$ to $\mathcal{O}(N\log(N))$, using the fact that $p_{max}\,q_{max} = \mathcal{O}(N)$. Afterwards, the obtained elements still need to be assigned to the corresponding matrix entries. As can be seen in Table I, the matrix inversion time becomes significant in the accelerated MoM code. Using those techniques, the spectral current associated with the excitation of the reference feed has been obtained in a few seconds and is illustrated in Fig. 4. Such result could not be obtained efficiently with HFSS as the solution of each periodic problem takes around 1 min with HFSS, compared with 25 ms using our MoM code, which corresponds to an acceleration by several orders of magnitude. The observed circles correspond to the SW propagating in the structure, as demonstrated in [28] for an infinite phased array of printed dipoles. The circles have a radius equal to $1.33k_0$, corresponding to the fundamental SW wavenumber, and are centered on the Floquet wavenumbers according to the periodicity of (15). That means, the coordinates of the centers of the circles are $(k_x^m, k_y^n) = (mk_0, 2nk_0)$, with $m$ and $n$ being arbitrary integers.

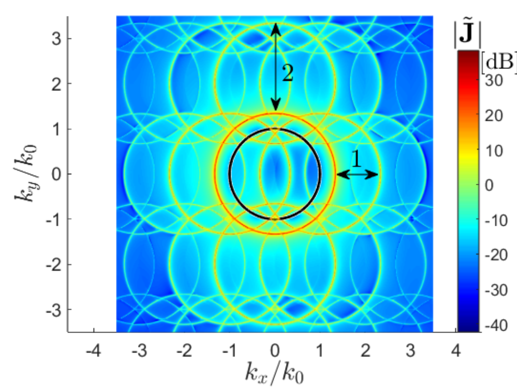


Fig. 4. Spectral current obtained with (15), for excitation of the reference feed only. The inner black circle delimits the visible region.

## V. Conclusion

An effective MoM formulation is proposed for the analysis of arbitrarily modulated MTS antennas with PBC. Owing to the adopted set of basis functions, and the proposed FFT-based acceleration techniques, the computational complexity has been dramatically reduced. The proposed methodology has been validated using the commercial software HFSS, and has been shown to be much more efficient than the latter. Further works may rely on the developed simulation tool to design sparse-array MTS antennas with beam scanning capability.

## ACKNOWLEDGMENT

The authors would like to thank Louis Delait from UCLouvain for his help with the HFSS simulations.

## REFERENCES

[1] B. H. Fong, J. S. Colburn, J. J. Ottusch, J. L. Visher, and D. F. Sievenpiper, "Scalar and tensor holographic artificial impedance surfaces," *IEEE Trans. Antennas Propag.*, vol. 58, no. 10, pp. 3212–3221, Jul. 2010.

[2] A. M. Patel and A. Grbic, "A printed leaky-wave antenna based on a sinusoidally-modulated reactance surface," *IEEE Trans. Antennas Propag.*, vol. 59, no. 6, pp. 2087–2096, Jun. 2011.

[3] G. Minatti, M. Faenzi, E. Martini, F. Caminita, P. De Vita, D. González-Ovejero, M. Sabbadini, and S. Maci, "Modulated metasurface antennas for space: Synthesis, analysis and realizations," *IEEE Trans. Antennas Propag.*, vol. 63, no. 4, pp. 1288–1300, Apr. 2015.

[4] G. Minatti, S. Maci, P. De Vita, A. Freni, and M. Sabbadini, "A circularly-polarized isoflux antenna based on anisotropic metasurface," *IEEE Trans. Antennas Propag.*, vol. 60, no. 11, pp. 4998–5009, Nov. 2012.

[5] M. Bodehou, A. Guth, K. A. Khalifeh, D. Heberling, and C. Craeye, "Multi-feed metasurface antennas: Direct numerical design and experimental validations," *IEEE Access*, vol. 11, pp. 35 754–35 762, Apr. 2023.

[6] G. Minatti, F. Caminita, E. Martini, M. Sabbadini, and S. Maci, "Synthesis of modulated-metasurface antennas with amplitude, phase, and polarization control," *IEEE Trans. Antennas Propag.*, vol. 64, no. 9, pp. 3907–3919, Sep. 2016.

[7] M. Bodehou, K. A. Khalifeh, S. N. Jha, and C. Craeye, "Direct numerical inversion methods for the design of surface wave-based metasurface antennas: Fundamentals, realizations, and perspectives," *IEEE Antennas Propag. Mag.*, vol. 64, no. 4, pp. 24–36, Aug. 2022.

[8] R. F. Harrington, "Field computation by moment methods," *Wiley-IEEE Press*, 1993.

[9] D. González-Ovejero and S. Maci, "Gaussian ring basis functions for the analysis of modulated metasurface antennas," *IEEE Trans. Antennas Propag.*, vol. 63, no. 9, pp. 3982–3993, Sep. 2015.

[10] M. A. Francavilla, E. Martini, S. Maci, and G. Vecchi, "On the numerical simulation of metasurfaces with impedance boundary condition integral equations," *IEEE Trans. Antennas Propag.*, vol. 63, no. 5, pp. 2153–2161, May 2015.

[11] M. Bodehou, D. González-Ovejero, C. Craeye, and I. Huynen, "Method of moments simulation of modulated metasurface antennas with a set of orthogonal entire-domain basis functions," *IEEE Trans. Antennas Propag.*, vol. 67, no. 2, pp. 1119–1130, Feb. 2019.

[12] D. Pozar, "Input impedance and mutual coupling of rectangular microstrip antennas," *IEEE Trans. Antennas Propag.*, vol. 30, no. 6, pp. 1191–1196, Nov. 1982.

[13] D. Pozar, S. Targonski, and H. Syrigos, "Design of millimeter wave microstrip reflectarrays," *IEEE Trans. Antennas Propag.*, vol. 45, no. 2, pp. 287–296, Feb. 1997.

[14] R. Mittra, C. Chan, and T. Cwik, "Techniques for analyzing frequency selective surfaces-a review," *Proceedings of the IEEE*, vol. 76, no. 12, pp. 1593–1615, Dec. 1988.

[15] J. Dessy, M. Bodehou, J. Cavillot, and C. Craeye, "Sparse-array metasurface for beam scanning," *IEEE Trans. Antennas Propag.*, vol. 72, no. 10, pp. 8088–8093, Oct. 2024.

[16] C. Craeye and D. Gonzalez Ovejero, "A review on array mutual coupling analysis," *Radio Sci.*, vol. 46, no. 2, pp. 1–25, Apr. 2011.

[17] L. Trintinalia and H. Ling, "Integral equation modeling of multilayered doubly-periodic lossy structures using periodic boundary condition and a connection scheme," *IEEE Trans. Antennas Propag.*, vol. 52, no. 9, pp. 2253–2261, Sep. 2004.

[18] X. Dardenne and C. Craeye, "Method of moments simulation of infinitely periodic structures combining metal with connected dielectric objects," *IEEE Trans. Antennas Propag.*, vol. 56, no. 8, pp. 2372–2380, Aug. 2008.

[19] F. Capolino, C. Craeye, X. Radu, and A. G. Schuchinsky, "Fundamentals of method of moments for artificial materials," in *Theory and Phenomena of Metamaterials*. CRC Press, 2009, ch. 5.

[20] J. Dessy, M. Bodehou, and C. Craeye, "Method of moments for the two-dimensional analysis of array-fed metasurface antennas," in *2024 Int. Conf. Electromagn. Adv. Appl. (ICEAA)*, Oct. 2024, pp. 200–204.

[21] J. Córcoles, M. Camacho, and R. R. Boix, "NUFFT-accelerated spectral-domain MoM with asymmetric rooftop basis functions for multilayered structures with periodic metallizations," *IEEE Trans. Antennas Propag.*, vol. 72, no. 5, pp. 4420–4430, May 2024.

[22] C. Chan, "A numerically efficient technique for the method of moments solution of electromagnetic problem associated with planar periodic structures," *Microw. Opt. Technol. Lett.*, vol. 1, no. 10, pp. 372–3745, Dec. 1988.

[23] J. Cavillot, M. Bodehou, and C. Craeye, "Metasurface antennas design: full-wave feeder modeling and far-field optimization," *IEEE Trans. Antennas Propag.*, vol. 71, no. 1, pp. 39–49, Jan. 2023.

[24] K. Michalski and J. Mosig, "Multilayered media Green's functions in integral equation formulations," *IEEE Trans. Antennas Propag.*, vol. 45, no. 3, pp. 508–519, Mar. 1997.

[25] N. Das and D. Pozar, "A generalized spectral-domain Green's function for multilayer dielectric substrates with application to multilayer transmission lines," *IEEE Trans. Microw. Theory Techn.*, vol. 35, no. 3, pp. 326–335, Mar. 1987.

[26] C. Shannon, "Communication in the presence of noise," *Proceedings of the IRE*, vol. 37, no. 1, pp. 10–21, Jan. 1949.

[27] E. T. Whittaker, "On the functions which are represented by the expansions of the interpolation-theory," *Pro. Roy. Soc. Edinburgh*, vol. 35, p. 181–194, Jul. 1915.

[28] D. Pozar and D. Schaubert, "Scan blindness in infinite phased arrays of printed dipoles," *IEEE Trans. Antennas Propag.*, vol. 32, no. 6, pp. 602–610, Jun. 1984.